COMPDYN 2011
3rd ECCOMAS Thematic Conference on
Computational Methods in Structural Dynamics and Earthquake Engineering
M. Papadrakakis, M. Fragiadakis, V. Plevris (eds.)
Corfu, Greece, 25–28 May 2011

THE CHALLENGES ASSOCIATED WITH THE INTRODUCTION OF A FREQUENCY DEPENDENT COUPLING INTO A PHENOMENOLOGICAL MODEL FOR VORTEX-INDUCED VIBRATION

R.H.M. Ogink[1] **and A.V. Metrikine**[2]

[1] Heerema Marine Contractors
Vondellaan 55, 2332 AA Leiden, The Netherlands
e-mail: rogink@hmc-heerema.com

[2] Delft University of Technology, Faculty of Civil Engineering and Geosciences
Stevinweg 1, 2628 CN Delft, The Netherlands
e-mail: a.metrikine@tudelft.nl

Keywords: Vortex-induced vibration, nonlinear dynamics, wake oscillator, frequency dependent coupling, fluid-structure interaction.

Abstract. *The aim of this paper is to improve the wake oscillator concept for the modeling of vortex-induced vibration of an elastically mounted cylinder in a fluid flow. To this end an attempt is made to introduce a coupling term in the wake oscillator model, that is based on a set of frequency dependent coefficients. Theoretically, it should be possible to determine these coefficients on the basis of so-called forced vibration measurements. In doing so a number of challenges are encountered. A consistent set of frequency dependent coefficients should conform to the forced vibration experiments at all amplitudes of cylinder motion and additionally it should satisfy the Kramers-Kronig relations. It has been found that it is not possible to find a set of frequency dependent coefficients with the wake oscillator model at hand that satisfies these requirements. The sensitivity of the frequency dependent coefficients to the presence of the dominant non-linearity in the wake oscillator at hand has been examined. On the basis of this analysis a new form for the wake oscillator model has been proposed.*

1 INTRODUCTION

1.1 Vortex-induced vibration

Flow over a bluff cylinder separates and vortices are formed in the wake behind the cylinder. The alternate shedding of these vortices results in an oscillating cross-flow force on the cylinder. The shedding frequency of the vortices follows the Strouhal relation and increases with increasing flow velocity. If the cylinder is mounted flexibly and the frequency of vortex shedding is close to the resonance frequency of the mounted system, the cylinder will start to vibrate in cross-flow direction. With an increase of the flow velocity the vortex shedding frequency does no longer follow the Strouhal relation, but *locks onto* the resonance frequency of the cylinder, thereby causing violent vibration of the cylinder over a wide range of flow velocities. This phenomenon is known as vortex-induced vibration (VIV). The occurrence of VIV can cause severe fatigue problems for long cylindrical structures that are exposed to air or water flow such as chimneys, railroad contact wires, the cables of stay bridges and free-hanging offshore pipelines. Recent reviews on VIV have been given by Sarpkaya [1] and Williamson and Govardhan [2].

1.2 VIV experiments

Vortex-induced vibration experiments on rigid, spring mounted cylinders can be divided into two groups, the so called *free* and *forced vibration* experiments. In a typical free vibration experiment a flexibly mounted rigid cylinder is placed in a wind tunnel or water channel. For a range of flow velocities V, the amplitude $\hat{y}$ and the frequency $f_c = \omega_c/(2\pi)$ of cylinder motion are measured. Results of two free vibration experiments performed by Khalak and Williamson [3] are plotted in Figs. 1 and 2. In these figures the flow velocity has been made non-dimensional by dividing it by the natural frequency of the spring mounted cylinder f_n and by the cylinder diameter D, that is, $V_n = V/f_n/D$. The frequency f_n is given by: $f_n = \sqrt{(k/m)}$, in which k is the spring stiffness of the mounted system and m the cylinder dry mass.

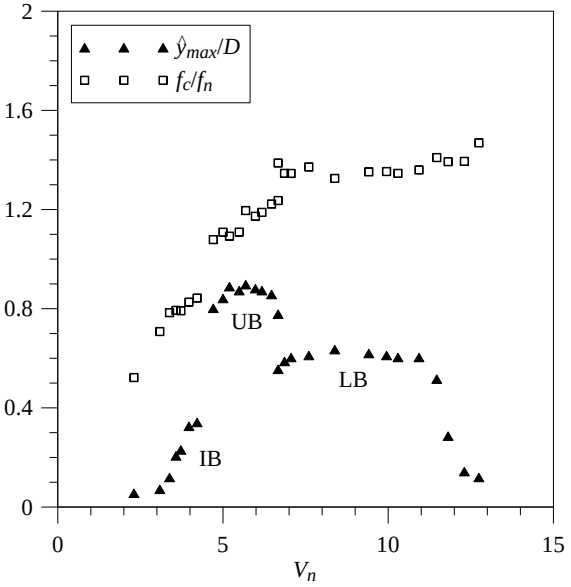

Figure 1: Amplitude and frequency of cylinder motion from the measurements of Khalak et al. [3] for $m^* = 2.4$.

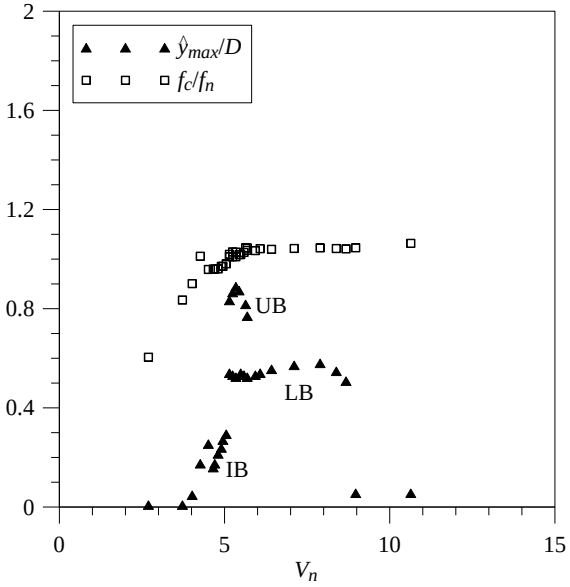

Figure 2: Amplitude and frequency of cylinder motion from the measurements of Khalak et al. [3] for $m^* = 20.6$.

The amplitude plot in Figs. 1 and 2 consists of three distinct branches, the initial, upper and lower branch, that have been marked IB, UB and LB, respectively. In the upper branch the frequency of vortex shedding f_s is very close to the natural frequency of the mounted cylinder, resulting in the cylinder motion with the largest amplitude. The frequency of vortex shedding is given by the Strouhal relation $f_s = \mathrm{St} \cdot V/D$, in which St denotes the Strouhal number. The upper branch is found for $f_s \approx f_n$ and since $\mathrm{St} \approx 0.2$, this takes place when $V_n \approx 1/\mathrm{St} \approx 5$. In the lower branch the amplitude of cylinder motion is constant over a range of flow velocities. The vortex shedding frequency is locked-in with the frequency of cylinder motion. The width of the lock-in range is dependent on the mass ratio m^*, see Figs. 1 and 2. For lower mass ratios the lock-in range is wider. The mass ratio is defined as the ratio of the cylinder mass and the mass of the displaced fluid: $m^* = 4m/(\pi\rho D^2 L)$, in which ρ denotes the density of the fluid and L the length of the cylinder.

Whereas in free vibration experiments, the coupled cylinder-fluid system sets its own frequency and amplitude, in forced vibration experiments amplitude and frequency are forced onto the system. In these experiments a cylinder is placed in a flow while it is at the same time being forced to vibrate sinusoidally in cross-flow direction with an amplitude $\hat{y}$ and a frequency $f_c = \omega_c/(2\pi)$. Typically the fluid force on the cylinder in cross-flow direction $F_y^y = \frac{1}{2}\rho D V^2 L C_y^y$ and in in-line direction $F_x^y = \frac{1}{2}\rho D V^2 L C_x^y$ are measured. In our notation C_y^y and C_x^y denote the non-dimensional fluid forces. To prevent confusion the following notation will be used consistently:

- A subscript ‘x’ or ‘y’ denotes the direction in which the fluid force is measured.
- A circumflex ‘^’ denotes an amplitude or a processed coefficient.
- A superscript ‘x’ or ‘y’ denotes the direction in which the cylinder is forced to vibrate in the forced vibration experiment. A superscript ‘0’ denotes a stationary cylinder.
- A second subscript ‘0’, ‘1’,’2’, etc. denotes the harmonic component for which the Fourier coefficient of the forced vibration time series has been determined.

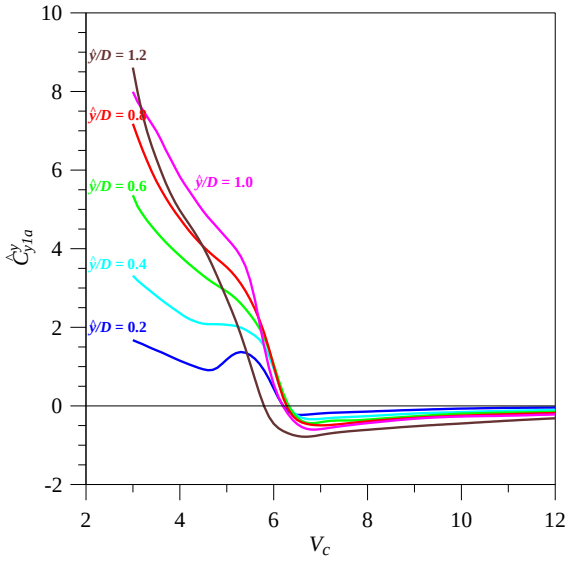

Figure 3: The cross-flow fluid force component in-phase with the cylinder acceleration from the measurements of Gopalkrishnan [4, 5].

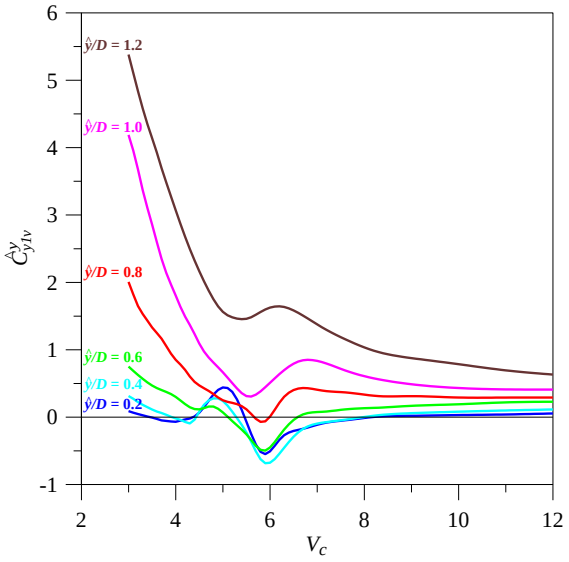

Figure 4: The cross-flow fluid force component in-phase with the cylinder velocity from the measurements of Gopalkrishnan [4, 5].

In Fig. 3 and 4, some of the results of the forced vibration measurements of Gopalkrishnan are depicted. These results have been reported in his PhD thesis [4], as well as in [5]. Gopal-

krishnan measured the fluid forces on a cylinder that was pulled through a water channel and at the same time was forced to vibrate in cross-flow direction. The motion of the cylinder is given by:

$$y = \hat{y}\sin(\omega_c t) \tag{1}$$

Among other results he reported in his thesis, for a range of forced amplitudes and forced frequencies, the constant fluid force coefficient in x-direction $\hat{C}^y_{x0}$ and the fluid force coefficient at the first harmonic in y-direction $\hat{C}^y_{y1}$. He decomposed $\hat{C}^y_{y1}$ in a part in-phase with the cylinder acceleration (or in anti-phase with the cylinder displacement): $\hat{C}^y_{y1a}$, depicted in Fig. 3, and a part in phase with the cylinder velocity: $\hat{C}^y_{y1v}$, depicted in Fig. 4. The flow velocity in Figs. 3 and 4 is made non-dimensional by dividing it by the cylinder diameter and the frequency of forced vibration: $V_c = V/f_c/D$. Approximating C^y_y with only the first Fourier component, results in:

$$\begin{aligned} C^y_y &\approx \hat{C}^y_{y1}\sin(\omega_c t + \varphi) = \hat{C}^y_{y1}\cos(\varphi)\sin(\omega_c t) + \hat{C}^y_{y1}\sin(\varphi)\cos(\omega_c t) \\ &= \hat{C}^y_{y1a}\sin(\omega_c t) - \hat{C}^y_{y1v}\cos(\omega_c t) \end{aligned} \tag{2}$$

1.3 Semi-empirical modeling of VIV

For the description of VIV engineers rely mainly on semi-empirical models, as Computational Fluid Dynamics (CFD) codes are still computationally too expensive for the determination of fluid forces on long cylinders such as the vertical riser pipelines at sea, that are being used in the offshore oil industry. These risers can have unsupported lengths of up to 2000 meters.

The semi-empirical models can be divided into two types. The first type of semi-empirical modeling consists of applying the fluid forces measured in forced vibration experiments directly on the right-hand side of the structural equation of motion. As the force coefficient $\hat{C}^y_{y1v}$ is in phase with the cylinder velocity, it acts as an added damping force. So in this model cylinder motion is possible when $\hat{C}^y_{y1v} < 0$. Since it is not known in advance with which amplitude and frequency the cylinder will vibrate and hence which values of $\hat{C}^y_{y1a}$ and $\hat{C}^y_{y1v}$ from the measurements have to be taken, an iterative procedure is needed. The drawback of this method is that it relies on the assumption that there will be a dominant mode of vibration, as the measurements that are being used have been carried out at a single frequency of forced vibration. This assumption is questionable in the case of very long pipes, such as the deepwater risers mentioned before. These pipes have a dense spectrum of resonance frequencies and will vibrate in a combination of several modes together. The presence of a sheared incoming flow will increase the complexity of finding the dominant modes even further.

The second type of semi-empirical model is the so-called oscillator model. In this type of model, the oscillating lift force is modeled by a non-linear oscillator equation, which contains a limit cycle, so that for a stationary cylinder an oscillating lift force is found. Oscillator equations that are commonly used are the Van der Pol equation and the Rayleigh equation. A Van der Pol equation that could be used is:

$$\ddot{C}_y + \varepsilon\omega_s\dot{C}_y\left(C_y^2 - \tfrac{1}{4}\hat{C}^2_{y1}\right) + \omega_s^2 C_y = A\frac{\ddot{y}}{D} + \omega_s B\frac{\dot{y}}{D}\ , \tag{3}$$

where $\hat{C}_{y1}^{0}$ is the amplitude of the limit cycle of the unforced oscillator, which should be equal to the cross-flow fluid force coefficient at the first harmonic on a stationary cylinder, $\omega_s = 2\pi f_s$ is the vortex shedding frequency, ε is a non-dimensional tuning parameter and overdots denote derivatives with respect to time t. The right-hand side of eq. (3) models the coupling between the structural displacement y and the fluid and contains the constant non-dimensional coupling coefficients A and B.

When the model predictions are compared with free vibration experiments, it is found that the oscillator model can produce acceptable results for structures experiencing VIV in air, in which the mass ratio of the structure and the surrounding fluid is high. A major drawback of most of the existing oscillator models is however that they do not scale correctly with the mass ratio and the damping ratio of the structure and the surrounding fluid. This means that these models have to be tuned separately for every possible combination of mass and damping ratio. This severely limits the predictive capabilities of these models. Moreover, existing oscillator models are not capable of describing the amplitude branches as found in the free vibration experiments at low mass ratios and hence underpredict the amplitude of the upper branch. Because of these shortcomings oscillator models are seldom used for engineering applications.

Oscillator models do have the favorable characteristic that they do not require an assumption of a dominant frequency. They consist of a system of coupled differential equations that can simply be solved in the time domain without any initial guess of frequency or amplitude. An oscillator model that can produce acceptable results over a range of mass and damping ratios on the basis of one set of tuning parameters, could therefore be useful as an engineering tool as it can deal with motion at multiple frequencies in a computationally inexpensive manner.

In [6], we have improved the existing oscillator model of Facchinetti et al. [7] by taking account of the relative velocity between cylinder and fluid. Subsequently, we tried to improve this model by making the coupling coefficients A and B frequency dependent by means of introducing a convolution integral into the time-domain model. We strived to derive a model that scales correctly with mass ratio, can describe the results of the forced vibration measurements and can describe the upper and lower branch of free vibration. We found, however, that with using a Van der Pol or Rayleigh equation and by trying to determine the frequency dependencies of A and B on the basis of the forced vibration measurements of Gopalkrishnan, we could not find a set of consistent frequency dependencies that could be used to determine the convolution kernel that is needed. The frequency dependencies appeared to be very sensitive to the non-linearities that are present in the model.

1.4 Objective of this paper

In this paper we will give a description of the challenges that are associated with the inclusion of a frequency dependent coupling between wake and structural oscillator. Specifically, we will focus on the sensitivity of the frequency dependencies to the presence of the non-linearity in the wake oscillator. On the basis of the results, we will make a first attempt at improving the existing model.

In Section 2, the wake oscillator model that will be used is discussed and the derivations that are needed, to include frequency dependent coupling coefficients in the wake oscillator, are given. In Section 3, the frequency dependent coefficients A and B are determined and the sensitivity of these coefficients to the presence of the non-linearity in the wake oscillator is investigated and on the basis of the results of this, in Section 4 a new wake oscillator model is proposed. The conclusions are presented in Section 5.

2 WAKE OSCILLATOR MODEL WITH FREQUENCY DEPENDENT COUPLING

2.1 The wake oscillator model

The wake oscillator model that will be used is based on the model of Facchinetti et al. [7] with the additional inclusion of the relative velocity between moving cylinder and fluid. Details of the model are given in [6]. The structural equation of motion is given by:

$$m\ddot{y} + b\dot{y} + ky = F_y, \tag{4}$$

in which b denotes the structural damping coefficient. The cross-flow fluid force F_y is assumed to consist of a part due to vortex shedding F_{VY} and a part due to potential added mass F_{AY}:

$$F_y = F_{VY} + F_{AY} = \tfrac{1}{2}\rho D V^2 L\, C_{VY} - m_a \ddot{y} \tag{5}$$

The potential added mass m_a is given by: $m_a = \hat{C}_a \pi \rho D^2 L$ /4, in which the potential added mass coefficient $\hat{C}_a$ has the value of 1.0. In [6] we have assumed that the non-dimensional cross-flow vortex force C_{VY} consists of a component C_{VD} in-line with the relative velocity $U = \sqrt{V^2 + \dot{y}^2}$ between moving cylinder and incoming flow and a component C_{VL} perpendicular to this relative velocity:

$$C_{VY} = \left(C_{VD} \sin\beta + C_{VL} \cos\beta\right) \frac{U^2}{V^2} \tag{6}$$

The angle β is the angle between the direction of the relative velocity and the horizontal. See Fig.5. It is given by:

$$\beta = -\arctan\left(\dot{y}/V\right), \quad \sin\beta = -\dot{y}/U = -\dot{y}\Big/\sqrt{V^2 + \dot{y}^2}, \quad \cos\beta = V/U = V\Big/\sqrt{V^2 + \dot{y}^2} \tag{7}$$

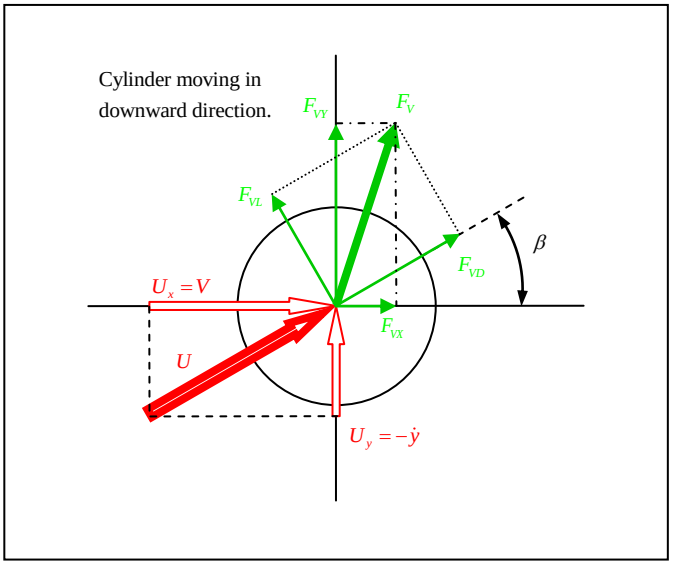

Figure 5: Definition of the angle and the decomposition of the vortex fluid force in drag, lift, horizontal and vertical direction

To complete the model description, the vortex force components C_{VD} and C_{VL} have to be defined. In [6] we have made the assumption that C_{VD} is constant and is equal to the mean drag force on a stationary cylinder and that C_{VL} can be calculated with a Van der Pol equation:

$$C_{VD} = \hat{C}^0_{x0} \tag{8}$$

$$\ddot{C}_{VL} + \varepsilon\,\omega_s\left(C_{VL}{}^2 - \tfrac{1}{4}(\hat{C}^0_{y1})^2\right)\dot{C}_{VL} + \omega_s^2 C_{VL} = \left(\frac{A}{D}\,\ddot{y} + \frac{B}{D}\,\omega_s \dot{y}\right)\cos\beta \tag{9}$$

The right-hand side of eq. (9) contains an acceleration coupling $A\ddot{y}$ and a velocity coupling $B\dot{y}$. Facchinetti et al. [7] have compared the differences on the free vibration modeling of using acceleration, velocity and displacement couplings and found that an acceleration coupling gave the best results. We have included the velocity coupling in eq. (9) for completeness, so that we have a coupling term $A\ddot{y}$ in (anti-)phase with the cylinder motion and a coupling term $B\dot{y}$ out-of-phase with the cylinder motion.

The constant coupling coefficients *A* and *B* will be made frequency dependent in Section 3. To this end we have pretuned the model to the free vibration measurements of Khalak et al. There are two ways to pretune the model. The first is to tune the model to the upper branch of free vibration and hope that by including the frequency dependencies the lower branch of free vibration can be described as well and the second way is to tune the model to the lower branch and hope that by including the frequency dependencies the upper branch can be described as well. We will call the first option *Case U* and the second one *Case L*. The values for the force coefficients $\hat{C}^0_{x0}$ and $\hat{C}^0_{y1}$ and the Strouhal number have been taken from the measurements of Gopalkrishnan.

To pretune the model, the coupled system consisting of the wake and structural oscillators, given by eq. (4) and (9) has been solved in the time domain with a fifth order Runge-Kutta routine. The initial conditions that have been used are $y(0) = \dot{y}(0) = \dot{C}_{VL}(0) = 0$ and $C_{VL}(0) = 0.01$. After a few periods of calculation the steady state is reached and the amplitude of cylinder motion has been determined by searching for the maximum recurring displacement and the frequency of cylinder motion has been determined by searching for the highest peak in the Fourier spectrum of the cylinder displacement. The results of the pretuning are presented in Figs. 6 and 7. In these figures solid lines depict results for increasing flow velocity and dashed lines results for decreasing flow velocity. The tuning parameters for the two cases are:

Case U:	***Case L:***
$\hat{C}^0_{x0} = 1.1856$	$\hat{C}^0_{x0} = 1.1856$
$\hat{C}^0_{y1} = 0.3842$	$\hat{C}^0_{y1} = 0.3842$
$\mathrm{St} = 0.1932$	$\mathrm{St} = 0.1932$
$A = 4.0 \cdot \dfrac{\hat{C}^0_{y1}}{2} = 0.7684$	$A = 12.0 \cdot \dfrac{\hat{C}^0_{y1}}{2} = 2.3052$
$B = 0$	$B = 0$
$\varepsilon = 0.05 \cdot \left(\dfrac{2}{\hat{C}^0_{y1}}\right)^2 = 1.3549$	$\varepsilon = 0.7 \cdot \left(\dfrac{2}{\hat{C}^0_{y1}}\right)^2 = 18.9690$

(10)

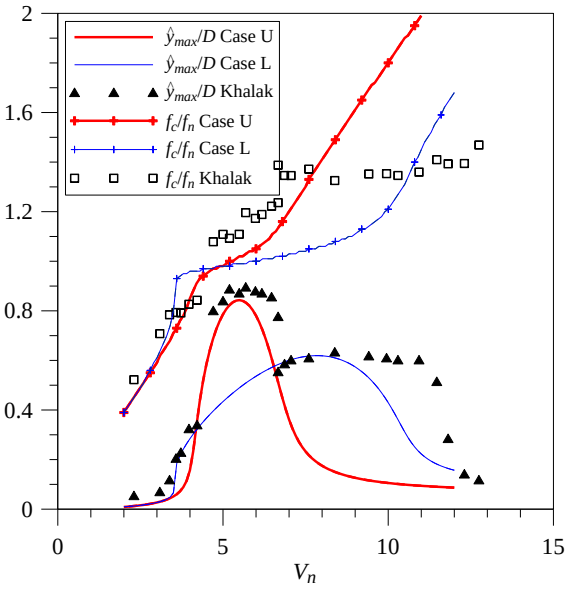

Figure 6: Pretuning of the wake oscillator model to the measurements of Khalak et al. [3] for $m^* = 2.4$.

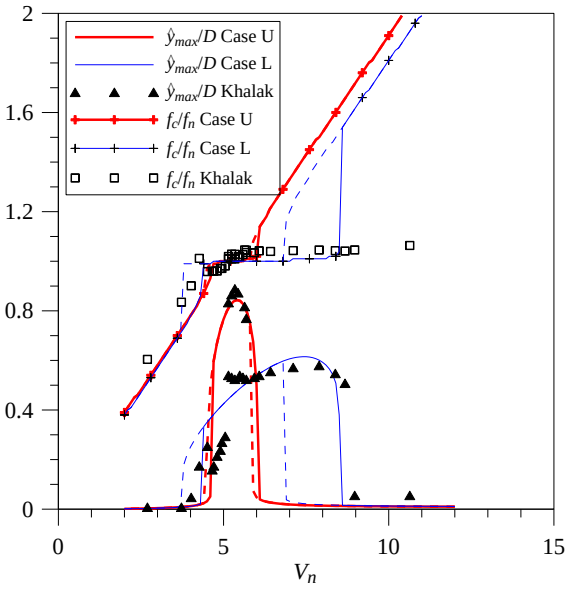

Figure 7: Pretuning of the wake oscillator model to the measurements of Khalak et al. [3] for $m^* = 20.6$.

2.2 Derivation of frequency dependent coupling

We strive to improve the wake oscillator presented in Section 2.1, by making the coupling coefficients functions of the cylinder frequency of vibration. These frequency dependent coefficients will be denoted by $\tilde{A}$ and $\tilde{B}$ for the moment. They will be determined over a range of cylinder frequencies on the basis of the forced vibration experiment of Gopalkrishnan, as will be explained in Section 3.1. The problem that is then encountered, is that if the coupled system consisting of the structural and wake oscillator is solved in the time domain, it is not known which values of the frequency dependent coefficients should be used, as the frequency of cylinder motion is not known in advance. The coupling term on the right-hand side of eq. (9) should therefore be replaced by a convolution integral. It is thus needed to derive the relation between the frequency dependent coefficients and the kernel of the convolution integral. To simplify the derivations, non-dimensional time $\tau = \omega_s t$ and non-dimensional cylinder frequency $\Omega_c = \omega_c/\omega_s$ are introduced. Substituting non-dimensional time into eq. (9) and dividing by ω_s^2 results in:

$$\frac{d^2C_{VL}}{d\tau^2} + \varepsilon\left(C_{VL}^2 - \tfrac{1}{4}(\hat{C}_{y1}^0)^2\right)\frac{dC_{VL}}{d\tau} + C_{VL} = \left(\frac{\tilde{A}}{D}\frac{d^2y}{d\tau^2} + \frac{\tilde{B}}{D}\frac{dy}{d\tau}\right)\cos\beta \tag{11}$$

Our goal is to replace the term $\frac{\tilde{A}(\Omega_c)}{D}\frac{d^2y}{d\tau^2} + \frac{\tilde{B}(\Omega_c)}{D}\frac{dy}{d\tau}$ in eq. (11) with the convolution $\frac{1}{D}\int_0^\tau K(\tau-\tilde{\tau})\frac{dy(\tilde{\tau})}{d\tilde{\tau}}d\tilde{\tau}$, in which $K(\tau)$ denotes the convolution kernel. The lower limit of integration starts at $\tilde{\tau} = 0$, as the cylinder cannot force the fluid, before it is moving itself. For large τ these two term should give the same results. This can be expressed as:

$$\begin{aligned}\frac{\tilde{A}(\Omega_c)}{D}\frac{d^2y}{d\tau^2}+\frac{\tilde{B}(\Omega_c)}{D}\frac{dy}{d\tau} &= \lim_{\tau\to\infty}\tfrac{1}{D}\int_0^{\tau}K(\tau-\tilde{\tau})\frac{dy(\tilde{\tau})}{d\tilde{\tau}}d\tilde{\tau}\\ &= \tfrac{1}{D}\int_0^{\infty}K(\tau-\tilde{\tau})\frac{dy(\tilde{\tau})}{d\tilde{\tau}}d\tilde{\tau}=\tfrac{1}{D}\int_0^{\infty}K(\tilde{\tau})\frac{dy(\tau-\tilde{\tau})}{d\tilde{\tau}}d\tilde{\tau}\end{aligned} \tag{12}$$

Substitution of the expression $y=\hat{y}\sin(\Omega_c\tau)$ results in the following relations:

$$\Omega_c\ \tilde{A}(\Omega_c)=-\int_0^{\infty}K(\tau)\sin(\Omega_c\tau)d\tau=A(\Omega_c) \tag{13}$$

$$\tilde{B}(\Omega_c)=\int_0^{\infty}K(\tau)\cos(\Omega_c\tau)d\tau=B(\Omega_c) \tag{14}$$

Eq. (13) and (14) show that, since $A(\Omega_c)$ and $B(\Omega_c)$ are the inverse sin- and cos-transform of the same kernel $K(\tau)$, these functions are not independent functions, but are in fact related to each other. This relation is known as the Kramers-Kronig relation. It can be expressed as follows, where attention has been paid to correctly include the boundaries at $\Omega=0$ and $\Omega\to\infty$:

$$\frac{A(\Omega)}{\Omega}-\lim_{\Omega\to\infty}\frac{A(\Omega)}{\Omega}=\frac{1}{\Omega}\frac{2}{\pi}\int_0^{\infty}\frac{\left(B(\tilde{\Omega})-B(\Omega)\right)\Omega}{\tilde{\Omega}^2-\Omega^2}d\tilde{\Omega} \tag{15}$$

$$B(\Omega)-B(0)=-\frac{2\Omega^2}{\pi}\int_0^{\infty}\frac{A(\tilde{\Omega})\big/\tilde{\Omega}-A(\Omega)\big/\Omega}{\tilde{\Omega}^2-\Omega^2}d\tilde{\Omega} \tag{16}$$

More details on the relations between $A(\Omega_c)$ and $B(\Omega_c)$ are given in [6].

3 DETERMINATION OF THE FREQUENCY DEPENDENT COEFFICIENTS *A*(Ω) AND *B*(Ω)

3.1 Method of determining the frequency dependent coefficients $A(\Omega_c)$ and $B(\Omega_c)$

It will be tried to determine the frequency dependent coefficients $A(\Omega_c)$ and $B(\Omega_c)$ on the basis of the forced vibration measurements of Gopalkrishnan. To this end, the forced vibration experiments need to be modeled with the wake oscillator model presented in Section 2. The forced vibration cross-flow fluid force C_y^y can be expressed as:

$$C_y^y=C_{VY}+C_{AY}=C_{VY}-\frac{m_a}{\frac{1}{2}\rho DV^2L}\ddot{y}, \tag{17}$$

in which C_{VY} is again given by eq. (6) :

$$C_{VY}=\left(C_{VD}\sin\beta+C_{VL}\cos\beta\right)\frac{U^2}{V^2} \tag{6}$$

By assuming a forced vibration in the form of: $y=\hat{y}\sin(\Omega_c\tau)$, the forced vibration coefficients $\hat{C}_{y1a}^y$ and $\hat{C}_{y1v}^y$ can be calculated with:

$$\begin{aligned}\hat{C}^{y}_{y1a} &= \frac{2}{\mathcal{T}_c}\int_{\tau_0}^{\tau_0+\mathcal{T}_c} C^{y}_{y}\sin\left(\Omega_c\tau\right)d\tau \\ &= \frac{2}{\mathcal{T}_c}\int_{\tau_0}^{\tau_0+\mathcal{T}_c} C_{VY}\sin\left(\Omega_c\tau\right)d\tau + \hat{C}_a 2\pi^3 \mathrm{St}^2{\Omega_c}^2\hat{y}/D\end{aligned} \tag{18}$$

$$\hat{C}^{y}_{y1v} = -\frac{2}{\mathcal{T}_c}\int_{\tau_0}^{\tau_0+\mathcal{T}_c} C^{y}_{y}\cos\left(\Omega_c\tau\right)d\tau = -\frac{2}{\mathcal{T}_c}\int_{\tau_0}^{\tau_0+\mathcal{T}_c} C_{VY}\cos\left(\Omega_c\tau\right)d\tau\,, \tag{19}$$

in which $\mathcal{T}_c = 2\pi/\Omega_c = 2\pi\omega_s/\omega_c$ is the non-dimensional period of forced vibration. The value of the component of the vortex fluid force in the direction of the relative velocity is again given by: $C_{VD} = \hat{C}^0_{x0}$. The component of the vortex fluid force perpendicular to the relative velocity will now be calculated with:

$$\frac{d^2C_{VL}}{d\tau^2} + \varepsilon\left({C_{VL}}^2 - \tfrac{1}{4}(\hat{C}^0_{y1})^2\right)\frac{dC_{VL}}{d\tau} + C_{VL} = \left(-\Omega_c A\frac{\hat{y}}{D}\sin(\Omega_c\tau) + \Omega_c B\frac{\hat{y}}{D}\cos(\Omega_c\tau)\right)\cos\beta \tag{20}$$

It is now possible to model the forced vibration with the help of eq. (6), (18), (19) and (20). By changing A and B in this model an error function will be minimized that characterizes the discrepancy between the model predictions and the measurements of Gopalkrishnan. The equations have been solved numerically in a similar manner as described in Section 2.1 with the value for ε and the initial values for A and B equal to the values given by (10). Then, the fluid force coefficients $\hat{C}^{y}_{y1a}$ and $\hat{C}^{y}_{y1v}$ have been calculated. When these values are known, the error can be determined as follows:

$$error = \left(\hat{C}^{y}_{y1a;\mathrm{model}} - \hat{C}^{y}_{y1a;\mathrm{measured}}\right)^2 + \left(\hat{C}^{y}_{y1v;\mathrm{model}} - \hat{C}^{y}_{y1v;\mathrm{measured}}\right)^2 \tag{21}$$

Subsequently, the error is minimized with a one-dimensional procedure that brackets the minimum and then performs a golden section search to find this minimum. This procedure is explained in detail by Press et al. in [8]. The procedure starts with changing A and keeping B constant and when under these conditions a minimum has been found, A is kept constant and B is changed. This is repeated over and over again until the error given by (21) is smaller than a preset value. Starting at V_c = 3 (with Ω_c = 1/St/V_c) and $\hat{y}/D$ = 0.2, the error is minimized until it is smaller than 10^{-6}. Then at the same amplitude the reduced velocity V_c is increased with dV_c = 0.1 and the calculations are repeated until the whole frequency range at this amplitude is covered, each time using the final A and B at the previous frequency as the initial values for the iterative procedure at the next frequency. In this manner the frequency dependent parameters $A(\Omega_c)$ and $B(\Omega_c)$ have been determined for the amplitudes of forced motion in the range of $\hat{y}/D$ = 0.2 to 1.2 with a step size of $d\hat{y}$ = 0.1·D.

3.2 Challenges involved in determining the coefficients $A(\Omega_c)$ and $B(\Omega_c)$

It is instructive at this point to state explicitly what the difficulties are in trying to determine the frequency dependent coefficients on the basis of the forced vibration experiments. Firstly, the frequency dependent coefficients will be determined for a number of amplitudes of forced vibration. But when modeling the free vibration with the wake oscillator containing the convolution integral, *one* kernel K based on only *one* set of frequency dependent curves $A(\Omega_c)$ and $B(\Omega_c)$ should be able to describe the fluid force behavior for all amplitudes of cy-

linder motion. This implies that for all amplitudes of forced vibration the same set of curves for $A(\Omega_c)$ and $B(\Omega_c)$ should be found.

Secondly, it has been shown in Section 2.2 that $A(\Omega_c)$ and $B(\Omega_c)$ are related through the Kramers-Kronig relations. It is not possible to determine $A(\Omega_c)$ and $B(\Omega_c)$ on the basis of the forced vibration measurements over the entire frequency range from zero to infinity, as the measurements have obviously been performed over a finite frequency range. For a set of frequency dependent coefficient $A(\Omega_c)$ and $B(\Omega_c)$ that is self-consistent, it should however be possible to extend these coefficient over the entire frequency range, such that the Kramers-Kronig relations are satisfied.

If we fail to find one set of coefficients $A(\Omega_c)$ and $B(\Omega_c)$ that are valid over a range of forced vibration amplitudes, or if the set of coefficients cannot be extended over the entire frequency range to satisfy the Kramers-Kronig relation, this will be an indication that the wake oscillator model does not contain the correct non-linearities.

3.3 Results of determining the coefficients $A(\Omega_c)$ and $B(\Omega_c)$ on the basis of forced vibration measurements

The frequency dependent curves that have been found for $A(\Omega_c)$ and $B(\Omega_c)$ with the method described in Section 3.1 are depicted in Fig. 8 and 9 for *Case U* and in Fig. 10 and 11 for *Case L*. It is clear from these figures that in both cases different curves for A and B are found at different amplitudes of forcing, implying that with the current model the results of Gopalkrishnan cannot be reproduced with a single set of frequency dependent parameters. It appears that the wake oscillator as tuned in *Case U* gives better results than as tuned in *Case L*, since in Fig. 8 and 9 the spread in the curves of $A(\Omega_c)$ and $B(\Omega_c)$ for different amplitudes is one order of magnitude smaller than in Fig. 10 and 11.

In [6], we have attempted to reduce the spread in the curves of $A(\Omega_c)$ and $B(\Omega_c)$ at different amplitudes of forcing in a number of ways. This included redefining the error function that has been used in the determination procedure, retuning the model by changing the parameter values given by eq. (10) and by replacing the Van der Pol-type non-linearity in eq. (20) with a Rayleigh-type non-linearity. None of these approaches reduced the spread in the curves of $A(\Omega_c)$ and $B(\Omega_c)$ to a significant degree.

Subsequently in [6], we have described a method based on complex curve fitting with a complex polynomial that should be able to, starting with a set of frequency dependent curves that are known over only a limited range of the frequency spectrum, expand this set over the entire spectrum such that the Kramers-Kronig relations are satisfied and the inverse transform of the coefficients $A(\Omega_c)$ and $B(\Omega_c)$ can be taken to determine the convolution kernel $K(\tau)$. We found that with this method we were not able to extend the curves for the amplitudes higher than $0.6 \cdot D$ over the entire spectrum and therefore we were not able to determine a convolution kernel on the basis of these curves. For the curves plotted in Figs. 8, 9, 10 and 11 at amplitudes of $0.6 \cdot D$ and lower, we were able to extend the curves over the entire spectrum, but this could only be done with a low order polynomial and therefore a poor fit to the curves used. After determining the convolution kernel $K(\tau)$ on the basis of one of these fits, the free vibration was modeled with inclusion of the convolution coupling. The results were very poor. See Fig. 10 in [6].

We therefore came to the conclusion that the wake oscillator model given by eq. (4), (6) and (9), with or without the convolution coupling, does not contain the correct non-linearities in either the damping term in eq. (9), the coupling term in eq. (9) or both. We also noted that the wake oscillator could possibly be improvement by adding an additional oscillator, so that the fluid force is modeled with a combination of two wake oscillators.

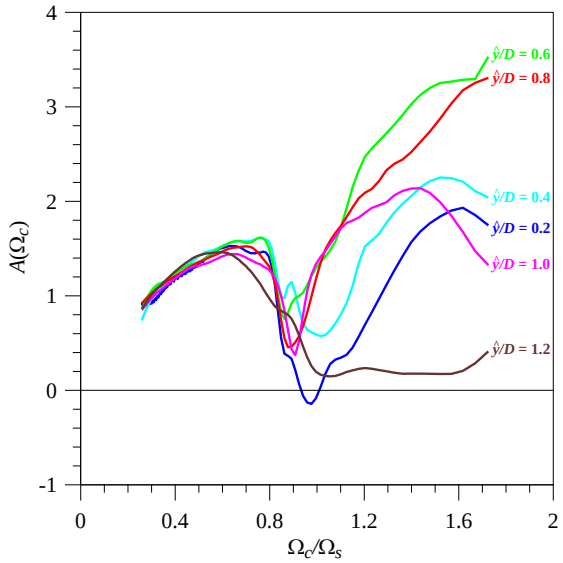

Figure 8: Curves found through a minimization procedure for the coefficient *A* for *Case U*.

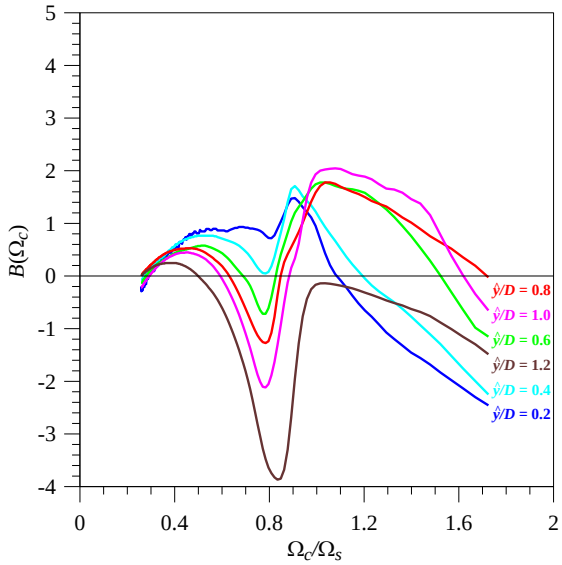

Figure 9: Curves found through a minimization procedure for the coefficient *B* for *Case U*.

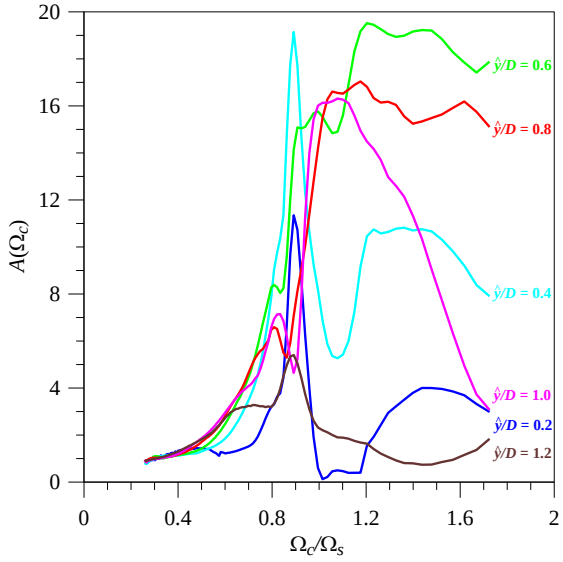

Figure 10: Curves found through a minimization procedure for the coefficient *A* for *Case L*.

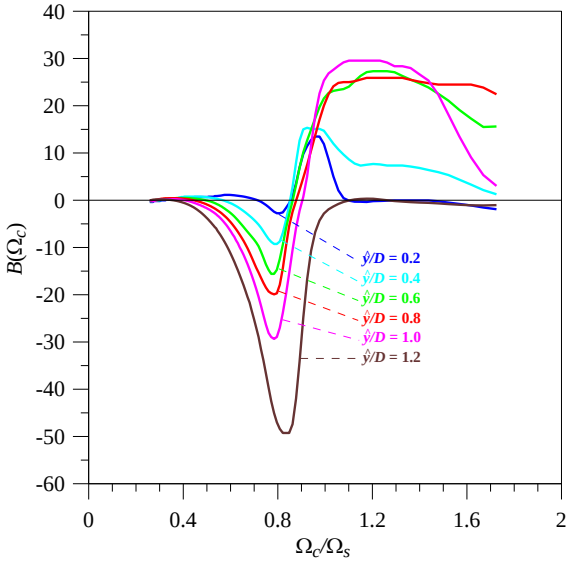

Figure 11: Curves found through a minimization procedure for the coefficient *B* for *Case L*.

3.4 Effect of removing the non-linearity in the damping term of the wake oscillator

It is remarkable that the spread in the curves for the frequency dependent coefficient at different amplitudes of forced vibration is an order of magnitude smaller for *Case U* compared to *Case L*. For *Case U*, the parameter ε, given by eq. (10), that multiplies the Van der Pol-type non-linearity in eq. (20) is on order of magnitude smaller compared to *Case L*. It seems, therefore, that the Van der Pol-type non-linearity in eq. (20) has a large influence on the spread of the frequency dependent curves found at different amplitudes of forced vibration. To explore whether this is indeed the case, the minimization procedure from Section 3.1 is repeated and the frequency dependent coefficients are determined anew, but in this case the non-linearity in the damping term in eq. (20) is replaced by a linear damping term:

$$\frac{d^2C_{VL}}{d\tau^2} + 2\,\varepsilon\,\frac{dC_{VL}}{d\tau} + C_{VL} = \left(-\Omega_c A \frac{\hat{y}}{D}\sin(\Omega_c\tau) + \Omega_c B \frac{\hat{y}}{D}\cos(\Omega_c\tau) \right)\cos\beta \tag{22}$$

We are fully aware that it is not possible to model the free vibration with eq. (22), as this equation does not contain a limit cycle and therefore cannot model the energy input from the fluid into the structural system at low amplitudes of motion, but we only wish to investigate the effects of the presence/non-presence of this non-linear damping term on the spread of the frequency dependent coefficient at different amplitudes of forced vibration.

The frequency dependent curves that have been found for $A(\Omega_c)$ and $B(\Omega_c)$ with the help of eq. (22) are depicted in Fig. 12 to 17 for three different values of the non-dimensional damping ratio ε, namely $\varepsilon = 0.5$, $\varepsilon = 0.3$ and $\varepsilon = 0.1$. It is immediately clear from Fig. 12 to 17, that the spread in the curves for $A(\Omega_c)$ and $B(\Omega_c)$ at different amplitudes of forced vibration is of the same order of magnitude as has been found for *Case U* in Section 3.3. For decreasing damping ratio ε, the spread in the curves reduces unmistakably. Only the curves for the highest amplitude of forced vibration $\hat{y}/D = 1.2$ does not collapse onto the other curves. But additional non-linearities in the coupled structure-fluid system that are not modeled with the equations used, will certainly be present in reality. These additional non-linearities will be most visible at the higher amplitudes of cylinder motion.

The fact that a much better correspondence of the frequency dependent curves at different amplitudes of forced vibration is found when the non-linearity in the damping term in the oscillator that describes C_{VL} is removed, leads to the conclusion that this non-linearity should most likely not be included at this place. The behavior of the oscillator that describes C_{VL} appears to be linear at low amplitudes of vibration. This means that the negative damping term that models the energy input from the fluid into the structural system should be placed at a different position in the coupled fluid-structure system.

4 A FIRST ATTEMPT AT A NEW WAKE MODEL CONTAINING MULTIPLE OSCILLATORS

Based on the findings of the previous section, a first attempt is made to develop a wake oscillator model in which the oscillator that describes C_{VL} is linear in first order approximation at low amplitudes of cylinder motion. We do not wish to derive a full model at this point that is able to describe both the free and forced vibration. It is only our objective here to investigate whether focusing our attention into this direction could be worthwhile. We start with the same basic equations as before and return to the usage of dimensional time t. The equations for the structural oscillator and the cross-flow fluid force do not change and are given by:

$$(m + m_a)\ddot{y} + b\dot{y} + ky = \tfrac{1}{2}\rho D V^2 L\, C_{VY} \tag{23}$$

$$C_{VY} = \left(C_{VD}\sin\beta + C_{VL}\cos\beta\right)\frac{U^2}{V^2} \tag{6}$$

It will still be assumed that: $C_{VD} = \hat{C}^0_{x0}$. For the force component C_{VL} the following equation is proposed of which the left-hand side is linear as discussed in Section 3.4:

$$\ddot{C}_{VL} + 2\varepsilon_L\,\omega_s\dot{C}_{VL} + \omega_s^2 C_{VL} = P_L\omega_s\,\dot{q} + \left(\frac{A_L}{D}\,\ddot{y} + \frac{B_L}{D}\,\omega_s\dot{y} + \frac{G_L}{D}\,\omega_s^2 y\right)\cos\beta\,, \tag{24}$$

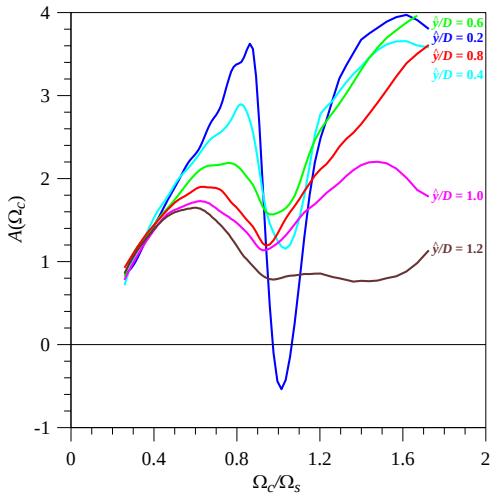

Figure 12: Curves found for the coefficient A for the linear case with $\varepsilon = 0.5$.

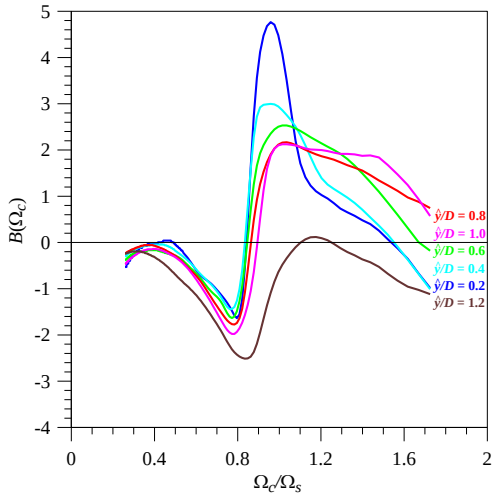

Figure 13: Curves found for the coefficient B for the linear case with $\varepsilon = 0.5$.

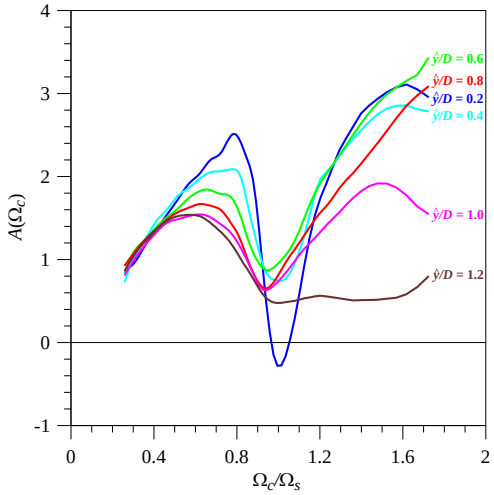

Figure 14: Curves found for the coefficient A for the linear case with $\varepsilon = 0.3$.

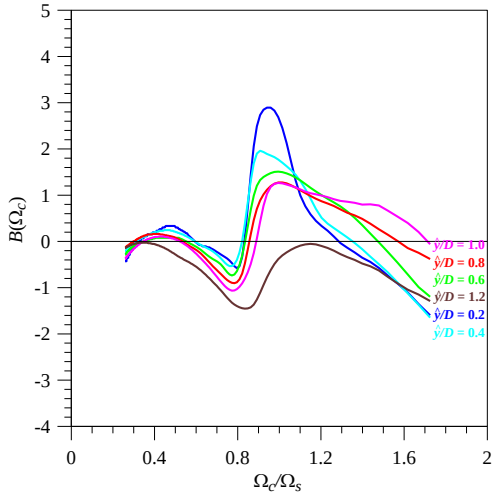

Figure 15: Curves found for the coefficient B for the linear case with $\varepsilon = 0.3$.

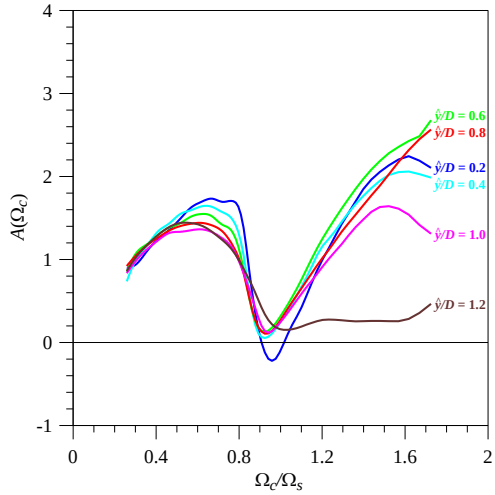

Figure 16: Curves found for the coefficient A for the linear case with $\varepsilon = 0.1$.

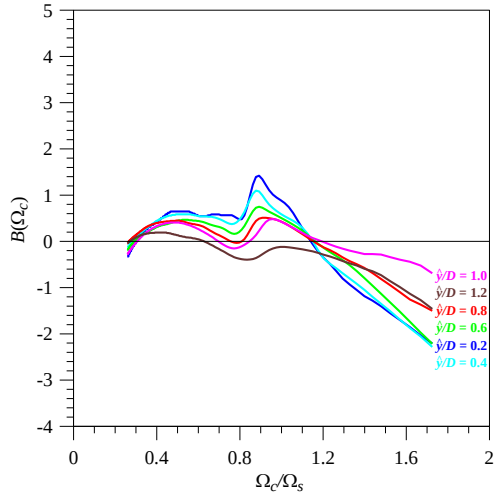

Figure 17: Curves found for the coefficient B for the linear case with $\varepsilon = 0.1$.

in which A_L, B_L, G_L and P_L are constant non-dimensional coupling coefficients and ε_L is the non-dimensional damping ratio. The non-linear damping term that is present in eq. (9) and that models the limit cycle of the cross-flow fluid force and hence the energy input from the fluid into the structural system, has been removed from eq. (24). Therefore a second oscillator is needed that reintroduces the limit cycle and thereby acts as forcing on eq. (24). The following form for this second oscillator is proposed:

$$\ddot{q} + \varepsilon_Q \, \omega_s (q^2 - 1) \, \dot{q} + \omega_s^2 q = \left(\frac{A_Q}{D} \, \ddot{y} + \frac{B_Q}{D} \, \omega_s \dot{y} + \frac{G_Q}{D} \, \omega_s^2 y \right) \cos \beta \,, \tag{25}$$

in which q is a wake variable that will be left undefined. A_Q, B_Q, and G_Q are constant non-dimensional coupling coefficients and ε_Q is a non-dimensional tuning parameter. To ensure that the cross-flow fluid force on a stationary cylinder as predicted by eq. (6) , (24) and (25) is equal to $\hat{C}_{y1}^0$, P_L should be equal to: $P_L = 2\varepsilon_L \hat{C}_{y1}^0 / 2 = \varepsilon_L \hat{C}_{y1}^0$.

The coupled system consisting of eq. (6), (23), (24) and (25) has been solved in the time domain and it has been tried to find values for the tuning coefficients A_L, B_L, G_L, ε_L, A_Q, B_Q, G_Q and ε_Q, such that results of the model would compare favorably with the free vibration measurements of Khalak et al. It has however been found that for the free vibration modeling this system of equations always overpredicted the amplitude of free vibration. This is likely caused by the removal of the Van der Pol-type nonlinearity from eq. (24). The presence of this term resulted in a strong damping at higher amplitudes of cylinder motion and it limited thereby the amplitude of cylinder motion that could be attained. This can be corrected by letting go of the assumption that: $C_{VD} = \hat{C}_{x0}^0$ and introducing an additional oscillator equation to describe C_{VD}. The presence of this additional oscillator will limit the amplitude of the cylinder motion. A suitable form for this oscillator is given by:

$$\ddot{C}_{VD} + 4\varepsilon_D \, \omega_s \dot{C}_{VD} + 4\omega_s^2 (C_{VD} - \hat{C}_{x0}^0) = P_D \omega_s \, q \, \dot{q} + \left(\frac{A_D}{D} \, \ddot{y} + \frac{B_D}{D} \, \omega_s \dot{y} + \frac{G_D}{D} \, \omega_s^2 y \right) \sin \beta \,, \tag{26}$$

in which A_D, B_D, G_D and P_D are constant non-dimensional coupling coefficients and ε_D is the non-dimensional damping ratio. The inclusion of eq. (26) into the model has the added advantage that it creates the possibility to also model the oscillating components of the drag force, which are known to oscillate at even multiples of the Strouhal frequency [1, 2]. To ensure that the oscillating component of the in-line fluid force on a stationary cylinder as predicted by the present system of equations is equal to the force component $\hat{C}_{x2}^0$ from the measurements of Gopalkrishnan, P_D should be equal to: $P_D = -16 \, \varepsilon_D \hat{C}_{x2}^0 / 4 = -4 \, \varepsilon_D \hat{C}_{x2}^0$.

Again, it has been tried to tune the system of equations, now given by eq. (6), (23), (24), (25) and (26) to the free vibration experiments of Khalak et al. The results of this attempt are depicted in Fig. 18 and 19. The following values for the tuning parameters have been used:

St = 0.1932, $\hat{C}_{x0}^0 = 1.1856$, $\hat{C}_{y1}^0 = 0.3842$, $\hat{C}_{x2}^0 = -0.0215$,
A_Q = 1.10, B_Q = -0.50, G_Q = 0.0, ε_Q = 0.10,
A_L = 0.70, B_L = 0.00, G_L = -1.15, ε_L = 0.30,
A_D = -8.00, B_D = -8.00, G_D = 5.00, ε_D = 0.30

It can be seen in Figs. 18 and 19 that the first results of the new wake model consisting of multiple oscillators seem to be very promising. It appears that with the help of multiple wake oscillators it is possible to describe the upper and lower branch of free vibration.

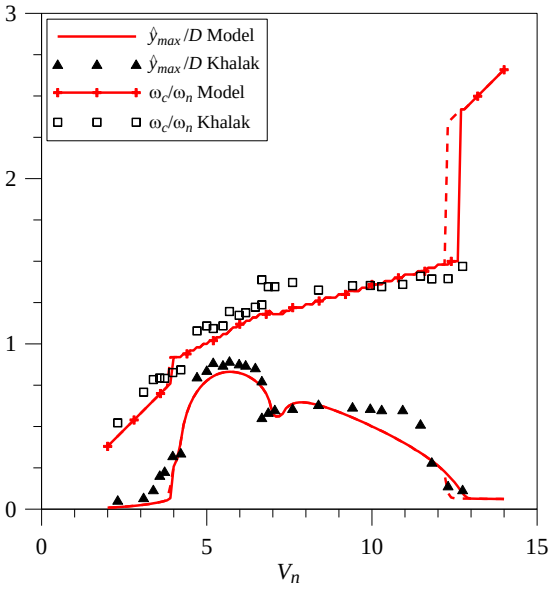

Figure 18: Comparison of the amplitude and frequency of oscillation of the multiple oscillator model with the measurements of Khalak et al. [3] for $m^* = 2.4$.

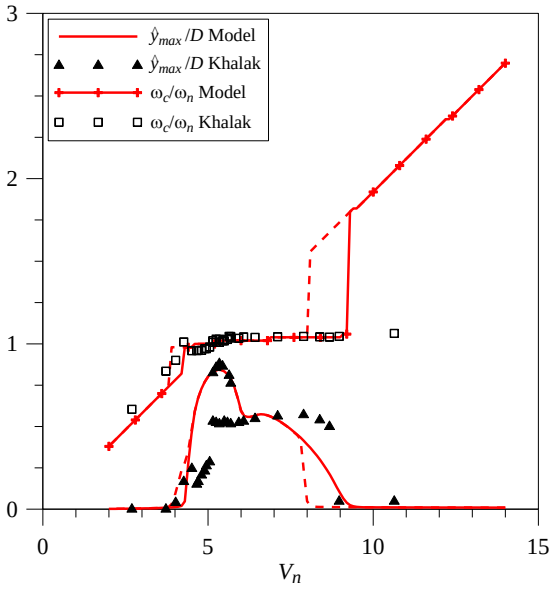

Figure 19: Comparison of the amplitude and frequency of oscillation of the multiple oscillator model with the measurements of Khalak et al. [3] for $m^* = 20.6$.

5 CONCLUSIONS

Starting with a wake oscillator model that has been developed earlier in [6] and [7] for the description of vortex-induced vibration, an attempt has been made to improve this model by making the coupling term between the structural and fluid oscillator frequency dependent. A set of consistent frequency dependent coupling coefficients is valid at all amplitudes of cylinder motion and satisfies the Kramers-Kronig relations. The frequency dependent coefficients have been determined on the basis of the results of a forced vibration experiment.

As reported earlier in [6], the sets of frequency dependent coefficients found at different amplitudes of forced cylinder motion do not correspond with each other and therefore fail the requirements mentioned above.

In this paper the influence of the presence of the dominant non-linearity in the wake oscillator on the discrepancy between the various sets of frequency dependent coefficients found at different amplitudes of cylinder motion has been examined. It has been found that removal of the dominant non-linearity reduced the discrepancy between the sets of frequency dependent coefficient.

Based on this result a new model is proposed consisting of linear oscillators for the components of the fluid forces due to vortex shedding. These oscillators are forced by the cylinder motion and a wake variable q, which is described by a Van der Pol equation. Preliminary results of this model seem to be promising.

REFERENCES

[1] T. Sarpkaya, A critical review of the intrinsic nature of vortex-induced vibrations. *Journal of Fluids and Structures*, **19**, 389-447, 2004.

[2] C.H.K. Williamson, R. Govardhan, Vortex-induced vibrations. *Annual Review of Fluid Mechanics*, **36**, 413-455, 2004.

[3] A. Khalak, C.H.K. Williamson, Motions, forces and mode transitions in vortex-induced vibrations at low mass-damping. *Journal of Fluids and Structures,* **13**, 813-851, 1999.

[4] R. Gopalkrishnan, *Vortex-induced forces on oscillating bluff cylinders, PhD Thesis*. Massachusetts Institute of Technology, 1992.

[5] F.S. Hover, A.H. Techet, M.S. Triantafyllou, Forces on oscillating uniform and tapered cylinders in crossflow. *Journal of Fluid Mechanics,* **363**, 97-114,1998.

[6] R.H.M. Ogink, A.V. Metrikine, A wake oscillator with frequency dependent coupling for the modeling of vortex-induced vibration. Journal of Sound and Vibration, **329**, 5452-5473, 2010.

[7] M.L. Facchinetti, E. de Langre, F. Biolley, Coupling of structure and wake oscillators in vortex-induced vibrations. Journal of Fluids and Structures, **19**, 123-140, 2004.

[8] W.H. Press, S.A. Teukolsky, W.T. Vetterling, B.P. Flannery, *Numerical recipes in Fortran77:The art of scientific computing, 2nd Edition*. Cambridge University Press, 1992.